



Steady flow past an elliptic cylinder inclined to the stream

S.C.R. DENNIS¹ and P.J.S. YOUNG²

¹*Department of Applied Mathematics, University of Western Ontario, London, Ontario, Canada N6A 5B7*

²*Defence Science and Technology Laboratory, Farnborough, GU14 0LX Hampshire, United Kingdom*

Received 29 July 2002; accepted in revised form 22 April 2003

Abstract. The properties of steady two-dimensional flow past an elliptic cylinder inclined to the oncoming stream are investigated for small to moderate values of the Reynolds number for which good accuracy can be assured. The solutions are based on a numerical method of solution of the Navier-Stokes equations for incompressible fluids which ensures that all the correct conditions of the problem are satisfied. In particular, the solution is carried out in such a way that the vorticity decays rapidly enough at large distances from the cylinder for the lift and drag on the cylinder to be finite. Results are presented for the variation of lift, drag and streamline patterns with inclination and Reynolds number. Two elliptic cylinders (based on their minor-to-major axes ratio) are considered. For an elliptic cylinder with minor-to-major axes ratio 1:5, results are obtained for Reynolds numbers up to 40 and inclination varying from zero to 90°. Streamline plots for these results show a development of the solution from asymmetric flow at zero inclination (with no separation), through asymmetric flows with increasing inclination (with either no separation, separation with a single recirculating region, or separation with two recirculatory regions) to the symmetric flow at 90° incidence (with two counter rotating vortices). Of interest are asymmetric steady-state results which contain two recirculatory regions trailing the cylinder, one attached and one unattached to the cylinder. Results are also obtained for a second elliptic cylinder with minor-to-major axes ratio 1:10 at Reynolds numbers 15 and 30, inclination 45°. These results are found to be in good agreement with corresponding unsteady results taken to long times (which are tending to a steady state).

Key words: elliptic cylinder, incompressible, steady, two-dimensional, viscous

1. Introduction

Despite the fact that the determination of the steady two-dimensional flow past an obstacle such as an elliptic cylinder or an aerofoil inclined to a uniform stream is one of the fundamental problems of fluid mechanics, there are surprisingly few results published of such studies for viscous incompressible fluids. There exist, of course, studies at very low Reynolds numbers based on Oseen's linearised equations, *e.g.* the analysis of Hasimoto [1] in the case of flow past an elliptic cylinder and studied more recently by Dennis and Kocabiyik [2]. For the full Navier-Stokes equations, however, there appear to be few results of investigations directed specifically at steady-state flow in cases where lift and circulation are present. An early paper by Mizomoto [3] has proposed a numerical method for solving problems of this nature and there have been a number of studies of steady-state flow past a rotating circular cylinder, of which the most recent are [4–8]. The paper by Badr *et al.* considered both steady and unsteady flow and was concerned principally with the problem of rectifying discrepancies found to exist between the calculated steady-state results of Ingham [5] at small Reynolds numbers and the corresponding results, at the same Reynolds numbers, obtained as the limit for large time of numerical solutions of the time-dependent equations. The discrepancies were rectified using methods which will be employed in the present paper. Ingham and Tang [7] also obtained

steady-state results in good agreement with those of Badr *et al.* [6]. Finally, D'Alessio and Dennis [9] have, subsequent to the initial analysis reported here, also considered steady flows including those past elliptic cylinders. They provide a comparison of their results to those reported here, for which there is excellent agreement. Their flow solution method was subsequently used to investigate forced convection from an elliptic cylinder in [10]. See also [11] for a study of flow past a flat plate of finite length.

A number of numerical solutions of the Navier-Stokes equations exist for unsteady flow past a cylinder inclined to the stream. Examples of these are the investigations of Lugt and Haussling [12], Panniker and Lavan [13] and Patel [14] for flow past an elliptic cylinder and Mehta and Lavan [15] for flow past a suddenly started aerofoil. Recently, Dennis, Nguyen and Kocabiyik [16] have studied the unsteady flow past a rotationally oscillating circular cylinder, while Kahawita and Wang [17] have considered the unsteady flow past a trapezoidal bluff cylinder. Generally speaking, these unsteady flow problems ultimately lead to solutions with vortex shedding, although Lugt and Haussling's solutions appeared to tend to a steady state for small Reynolds numbers. Panniker and Lavan find that their method gives a discontinuity of pressure on the surface of the cylinder which grows with time; this would complicate any attempt to obtain steady-state results by this method. The question of enforcing periodicity of the pressure round the contour of the cylinder, *i.e.*, that the pressure repeats itself after any complete circuit, was considered by Badr and Dennis [18] in the case of unsteady flow due to a rotating and translating circular cylinder. It was shown that periodicity was maintained provided that a condition involving a definite integral of the vorticity over the flow field was satisfied; this condition was utilised in the numerical procedure.

The steady-state flow past an elliptic cylinder inclined to the stream, so that lift and circulation are present, was investigated by Dennis [19]. From consideration of the flow at large distances, assumed to be governed by Oseen's linearised equations, it was shown that, although the decay of vorticity to zero at large distances from the cylinder was a necessary condition for an acceptable solution, it was not sufficient. In fact, the vorticity must decay fast enough by elimination of an unwanted term in the asymptotic solution. When this is eliminated, the pressure is single-valued, as required. On this basis, Badr *et al.* [6] employed scalings of the vorticity and stream function designed to eliminate the effect of the slowly decaying vorticity term, thus transforming the Navier-Stokes equations into suitable forms.

We employ the same method in the present paper to illustrate an acceptable method of obtaining solutions for steady-state flow past an elliptic cylinder inclined to the stream. Results are presented for two elliptic cylinders with the following minor-to-major axes ratios: 1:5 and 1:10. The Reynolds numbers are small, namely in the range 1 to 40 based on the length of the major axis of the cylinder. Such low-Reynolds-number flows are of interest since they cover the range of flight of many insects. The results obtained have been carefully tested for accuracy and a primary object has been to obtain an acceptable solution procedure. For the elliptic cylinder with minor-to-major axes ratio 1:5, lift, drag and other properties of the flow are calculated for a range of inclinations of the cylinder from zero to 90° and Reynolds number varying up to 40. These results indicate the onset of separation and stall as the inclination increases. Results for the second elliptic cylinder with minor-to-major axes ratio 1:10 are also obtained for Reynolds numbers 15 and 30, inclination 45° , allowing comparison with the quasi-steady results obtained by Lugt and Haussling [12] for the corresponding unsteady problem.

2. Basic equations and theory

We start with the Navier-Stokes equations for incompressible fluids in the dimensionless form

$$(\tilde{\mathbf{v}} \cdot \tilde{\nabla})\tilde{\mathbf{v}} = \frac{2}{\mathbf{R}}\tilde{\nabla}^2\tilde{\mathbf{v}} - \text{grad } p \quad (1)$$

for steady motion, where $\tilde{\mathbf{v}} = (u, v)$ is the velocity vector and p the pressure. The Reynolds number is defined by $\mathbf{R} = 2Ud/\nu$, where d is a representative dimension, ν is the dynamic viscosity of the fluid and U is the velocity of the undisturbed stream. Thus, as usual,

$$\tilde{\mathbf{v}} = \tilde{\mathbf{v}}^*/U, \quad (x, y) = (x^*, y^*)/d, \quad p = p^*/\rho U^2, \quad (2)$$

where the starred quantities are dimensional and ρ is the fluid density. The equation of continuity $\text{div } \tilde{\mathbf{v}} = 0$ is satisfied by the introduction of the usual dimensionless stream function ψ , which satisfies the equations

$$u = \partial\psi/\partial y, \quad v = -\partial\psi/\partial x. \quad (3)$$

We shall also work in terms of the customary scalar vorticity $\zeta = \partial v/\partial x - \partial u/\partial y$. The steady flow considered is that past an elliptic cylinder with major and minor axis lengths of $2a$ and $2b$, respectively, with the origin of coordinates (x, y) at the centre and major axis in the direction of x . The uniform stream makes an angle α with the positive direction of x .

The elliptic coordinate transformation is employed in the form

$$x = \cosh \xi \cos(\eta + \alpha), \quad y = \sinh \xi \sin(\eta + \alpha). \quad (4)$$

The orientation of these coordinates is such that the uniform stream coincides with $\eta = 0$ as $\xi \rightarrow \infty$. If the ellipse with semi-axes a and b is associated with $\xi = \xi_0$, then $\xi_0 = \tanh^{-1}(b/a)$. The dimensionless lengths of the major and minor axes are $2 \cosh \xi_0$ and $2 \sinh \xi_0$ respectively and it is convenient to define a Reynolds number

$$\text{Re} = (2Ud \cosh \xi_0)/\nu \quad (5)$$

based on the dimensional major axis; thus $\mathbf{R} = \text{Re}/\cosh \xi_0$ in (1).

In terms of the vorticity and stream function, the governing equations for the flow are

$$\frac{\partial^2 \zeta}{\partial \xi^2} + \frac{\partial^2 \zeta}{\partial \eta^2} = \frac{\mathbf{R}}{2} \left(\frac{\partial \psi}{\partial \eta} \frac{\partial \zeta}{\partial \xi} - \frac{\partial \psi}{\partial \xi} \frac{\partial \zeta}{\partial \eta} \right), \quad (6)$$

$$\frac{\partial^2 \psi}{\partial \xi^2} + \frac{\partial^2 \psi}{\partial \eta^2} + \frac{1}{2}(\cosh 2\xi - \cos 2(\eta + \alpha))\zeta = 0. \quad (7)$$

The boundary conditions are that

$$\begin{aligned} \psi = \partial\psi/\partial\xi = 0 \quad \text{when } \xi = \xi_0, \\ e^{-\xi} \partial\psi/\partial\xi \rightarrow \frac{1}{2} \sin \eta, \quad e^{-\xi} \partial\psi/\partial\eta \rightarrow \frac{1}{2} \cos \eta \quad \text{as } \xi \rightarrow \infty, \\ \psi(\xi, \eta) = \psi(\xi, \eta + 2\pi), \quad \zeta(\xi, \eta) = \zeta(\xi, \eta + 2\pi). \end{aligned} \quad (8a,b,c)$$

The conditions (8b) ensure that the velocity components of the motion tend to those of a uniform stream as $\xi \rightarrow \infty$. It follows also by (8b) that we must have

$$\zeta \rightarrow 0 \quad \text{as} \quad \xi \rightarrow \infty \quad (9)$$

but, while this is a necessary condition, it is not sufficient to obtain an acceptable solution.

We can see that this is the case by considering the limiting form of (6) as $\xi \rightarrow \infty$ obtained by linearising with the Equations (8b), which gives the equation

$$\frac{\partial^2 \zeta}{\partial \xi^2} + \frac{\partial^2 \zeta}{\partial \eta^2} = \frac{R}{4} e^\xi \left(\cos \eta \frac{\partial \zeta}{\partial \xi} - \sin \eta \frac{\partial \zeta}{\partial \eta} \right). \quad (10)$$

The solution must satisfy (9) and is found to be of the form

$$\zeta = e^{\lambda \cos \eta} \sum_{n=0}^{\infty} (a_n \cos n\eta + b_n \sin n\eta) K_n(\lambda), \quad (11)$$

where

$$\lambda(\xi) = \frac{1}{8} R e^\xi \quad (12)$$

and $K_n(\lambda)$ is the modified Bessel function of the second kind of order n . For large enough ξ we can replace $K_n(\lambda)$ by the leading term of its asymptotic expansion so that (11) may be written, approximately, in the form

$$\zeta \sim (2/\pi\lambda)^{1/2} e^{\lambda(\cos \eta - 1)} F(\eta), \quad (13)$$

where $F(\eta)$ is a function having the form

$$F(\eta) \sim A + B\eta, \quad \text{as} \quad \eta \rightarrow 0, \quad (14)$$

where A and B are constants. Thus, as $\xi \rightarrow \infty$, ζ is exponentially small except where $\lambda(\cos \eta - 1) = O(1)$, *i.e.*, where $\eta = O(\lambda^{-1/2})$. If we put $\eta = (2/\lambda)^{1/2} \varphi$ and neglect terms of order λ^{-1} in the exponent of the exponential in (13) as $\lambda \rightarrow \infty$, we obtain

$$\zeta \sim (A'\lambda^{-1/2} + B'\lambda^{-1}\varphi)e^{-\varphi^2} \quad \text{as} \quad \lambda \rightarrow \infty. \quad (15)$$

This derivation assumes, of course, that the coefficients a_n and b_n in (11) are such that certain infinite series are convergent in order that the constants A and B in (14) shall exist. However, Young [20] gives an alternative derivation in which the expression (11) is not utilised and such assumptions are not necessary. The essential point is that ζ is significant over some region defined by $0 \leq |\varphi| \leq K$, where K is a finite positive constant and that within this region the asymptotic decay of vorticity as $\lambda \rightarrow \infty$ is given by (15), so that $\zeta \rightarrow 0$ as $\lambda \rightarrow \infty$. However, the term multiplying A' in (15) is not acceptable since, if it is present, the viscous stresses are such that, as $\lambda \rightarrow \infty$, integration of them round a large contour surrounding the cylinder leads to infinite forces on the cylinder. A sufficient condition for an acceptable solution is therefore that $A' = 0$. The problem does not arise for flows which are symmetrical about $\eta = 0$, for in this case $A' \equiv 0$.

We may show that the term multiplying A' in (15) is unacceptable by considering the perturbation stream function Ψ defined by the equation

$$\psi = \Psi + \sinh \xi \sin \eta, \quad (16)$$

which satisfies the same equation (7) as ψ . Since, as $\xi \rightarrow \infty$, the vorticity is significant only in a type of boundary layer for which $\eta = (2/\lambda)^{1/2}\varphi$, it follows that the term $\partial^2\Psi/\partial\xi^2$ which would arise in (7) can be neglected compared with $\partial^2\Psi/\partial\eta^2$. This does not mean that $\partial^2\Psi/\partial\xi^2 \rightarrow 0$ as $\xi \rightarrow \infty$, certainly not within the region of significance of vorticity, but rather that $\partial^2\Psi/\partial\eta^2 = O(\lambda)$. It is then found that, in terms of Ψ and the coordinate φ , Equation (7) becomes as $\xi \rightarrow \infty$,

$$\frac{\partial^2\Psi}{\partial\varphi^2} + \frac{32}{R^2}(A'\lambda^{1/2} + B'\varphi)e^{-\varphi^2} + O(\lambda^{-1/2}) = 0, \quad (17)$$

where the expression (15) has been substituted for ζ .

With neglect of the $O(\lambda^{-1/2})$ term, Equation (17) may be solved by integrating twice with regard to φ . However, the resulting solution for Ψ contains an $O(\lambda^{1/2})$ term associated with the constant A' and it is this term which leads to an infinite lift and moment on the cylinder. If (X^*, Y^*) are the component forces in the x^* and y^* directions, respectively, we define dimensionless components by (X, Y) where

$$X^* = X\rho dU^2, \quad Y^* = Y\rho dU^2. \quad (18)$$

Then if C is any contour surrounding the cylinder we find

$$\begin{aligned} X &= -\oint_C \left\{ lp + \frac{2}{R}m\zeta + u(lu + mv) \right\} ds, \\ Y &= -\oint_C \left\{ mp - \frac{2}{R}l\zeta + v(lu + mv) \right\} ds, \end{aligned} \quad (19a,b)$$

where s is measured round the contour C in the anti-clockwise sense and (l, m) are the direction cosines of the outward normal to C . The lift and drag coefficients, defined respectively by

$$C_L = \frac{L}{\rho dU^2}, \quad C_D = \frac{D}{\rho dU^2} \quad (20)$$

in terms of the lift L and drag D , are then given by

$$C_L = Y \cos \alpha - X \sin \alpha, \quad C_D = X \cos \alpha + Y \sin \alpha. \quad (21)$$

We now use (19) and (21) and take the contour C to be large enough so that the expression (15) for ζ and the corresponding expression for Ψ found from (17) are valid. The pressure p may be found by substituting these asymptotic expressions for ζ and Ψ in the appropriate momentum equation and integrating along C from some base point. It is then found that the term associated with A' in C_L becomes infinite as the contour C becomes indefinitely large. This term must therefore be eliminated in any numerical procedure; in other words, the vorticity must not only decay to zero at large enough distances from the cylinder, but it must be made to decay rapidly enough by ensuring that $A' = 0$. This is achieved by suitable transformations of the vorticity and stream function in order to eliminate the slowly decaying terms present in the asymptotic expansions for these functions. This is briefly considered in the following sections. The asymptotic expression for Ψ obtained by integrating (17) twice with respect to φ with $A' = 0$ is found to be

$$\Psi \sim -\frac{1}{2}C_D \operatorname{erf} \varphi + \frac{C_D \varphi}{\pi \sqrt{2\lambda}} - \frac{C_L}{\pi} \log \left(\frac{1}{2} \sqrt{\frac{R}{\lambda}} \right), \quad (22)$$

where the arbitrary functions of λ which appear have been found by imposing continuity on Ψ at $\eta = \pm\pi$ and requiring Ψ to be harmonic outside the wake. These asymptotic results are in agreement with those derived by Imai [21], who used the Oseen type of successive approximation on the Navier-Stokes equations.

3. Method of solution

The numerical method is essentially the same as that used by Badr *et al.* [6] for determining the steady flow past a rotating circular cylinder. The essence is to adopt transformations of the variables given by

$$\psi = \Phi/z^2, \quad \zeta = z^2\chi, \quad z = e^{-\xi/2}. \quad (23)$$

The asymptotic expression (15) for ζ with $A' = 0$ and the corresponding expression for ψ obtained from (16) and (17) are then used as boundary conditions at some small enough value z_0 of z . The unknown constants in the asymptotic expressions can be evaluated in terms of the lift and drag coefficients C_L and C_D by integration round a large contour surrounding the cylinder. In terms of Φ and χ we find

$$\Phi \sim \frac{1}{2} \sin \eta - \frac{C_L}{\pi} z^2 \log(\sqrt{2z}) + \frac{1}{2} C_D z^2 \left(\frac{\eta}{\pi} - \operatorname{erf} \varphi \right) + \frac{\sqrt{R} C_D C_L}{2\pi^{3/2}} z^3 \log(\sqrt{2z}) e^{-\varphi^2}. \quad (24a)$$

$$\chi \sim -\frac{R C_D}{2\sqrt{\pi}} \varphi e^{-\varphi^2} - \frac{R^{3/2} C_D C_L}{4\pi^{3/2}} z \log(\sqrt{2z}) (2\varphi^2 - 1) e^{-\varphi^2}. \quad (24b)$$

Thus, if we enforce (24a,b) as boundary conditions on Φ and χ as $z \rightarrow 0$, then Φ remains finite and we suppress from χ the unwanted term which corresponds to that multiplying A' in (15). One may note that since this term is present in the asymptotic solution for ζ it can, unless successfully eliminated, exert an influence on the solution; in other words, inaccuracies in the numerical solution can give rise to the unwanted component in (15), with consequent unacceptable effects.

After transformation with (23), equations (6) and (7) become

$$z^2 \frac{\partial^2 \chi}{\partial z^2} + 5z \frac{\partial \chi}{\partial z} + 4 \frac{\partial^2 \chi}{\partial \eta^2} + 4\chi = \frac{R}{z} \left\{ \left(\frac{\partial \Phi}{\partial z} - \frac{2}{z} \Phi \right) \frac{\partial \chi}{\partial \eta} - \frac{\partial \Phi}{\partial \eta} \left(\frac{\partial \chi}{\partial z} + \frac{2}{z} \chi \right) \right\}, \quad (25)$$

$$z^2 \frac{\partial^2 \Phi}{\partial z^2} - 3z \frac{\partial \Phi}{\partial z} + 4 \frac{\partial^2 \Phi}{\partial \eta^2} + 4\Phi + H\chi = 0, \quad (26)$$

where $H = 1 + z^8 - 2z^4 \cos 2(\eta + \alpha)$. The boundary conditions are that

$$\Phi = \frac{\partial \Phi}{\partial z} = 0 \quad \text{when} \quad z = z_1, \quad (27)$$

where $z_1 = e^{-\xi_0/2}$ and Φ and χ are assumed to be given by (24) as $z \rightarrow 0$. In practice (24a,b) were applied at some value $z = z_0$ close enough to $z = 0$. The missing boundary condition at $z = z_1$ for χ which is necessary to treat (25) and (26) as complete boundary-value problems is found by satisfying (26) at the boundary and using (27). By means of a Taylor expansion at $z = z_1$ in which sufficient derivatives of Φ are taken into account, we may deduce the approximation

$$\chi(z_1, \eta) = \frac{-6z_1^2 \Phi(z_1 - h, \eta)/h^2 - H_1 \chi(z_1 - h, \eta)}{(2 - h/z_1)H_1 - h \left(\frac{\partial H}{\partial z} \right)_1}, \quad (28)$$

where $H_1 = H(z_1, \eta)$. This is of $O(h^2)$ accuracy and is equivalent to the approximation of Woods [22] in the case of the present equation (26).

The Equations (25) and (26) were solved by expressing all derivatives in terms of central differences at each internal point of a rectangular grid whose sides are parallel to the z and η directions.

The computational grid was broken into regions so that the grid size in the η direction was reduced as $z \rightarrow 0$. This was done to ensure sufficient grid points lie in the region of significant vorticity as $z \rightarrow 0$. From the asymptotic solution (24), the vorticity is confined as $z \rightarrow 0$ to a region for which $|\varphi| < K$, where K is a positive constant whose choice depends upon the degree of precision which it is desired to retain in the computed vorticity. Since this corresponds to a region for which $|\eta| < 2K(z/R)^{1/2}$, the grid size k in the η direction becomes too large in the neighbourhood of $z = 0$. This situation is dealt with by means of a sequence of grid reductions in the grid size k as $z \rightarrow 0$ in which the grid is successfully halved so as to retain approximately the same number of grid points in the computational domain $|\eta| < 2K(z/R)^{1/2}$. For $|\eta| > 2K(z/R)^{1/2}$ the vorticity may be assumed to be zero. The number of grid reductions necessary was found to depend upon Re and the choice of z_0 .

An iterative method was used for solving the finite-difference equations subject to their boundary conditions. This method was found to be satisfactory, with convergence being achieved in typically 10,000 to 15,000 iterations for a grid containing 40×160 points, run time being 100 to 150 seconds on a 333 MHz Pentium processor. More sophisticated methods, such as Newton's method used by Fornberg [23], could easily be applied to this problem with resulting increase in efficiency of solution.

The lift and drag coefficients required in (24) were calculated each iteration by integration round the cylinder surface using appropriate forms of (19) and (21). These coefficients may be decomposed into their pressure and friction components, *i.e.*,

$$C_L = C_{LP} + C_{LF}, \quad C_D = C_{DP} + C_{DF}. \quad (29a,b)$$

With the elliptic coordinate transformation (4), we find

$$\begin{aligned} C_{LP} &= -\frac{2 \cos \alpha \cosh^2 \xi_0}{Re} \int_0^{2\pi} \left(\frac{\partial \zeta}{\partial \xi} \right)_0 \cos(\eta + \alpha) d\eta - \frac{\sin \alpha \sinh 2\xi_0}{Re} \int_0^{2\pi} \left(\frac{\partial \zeta}{\partial \xi} \right)_0 \sin(\eta + \alpha) d\eta, \\ C_{LF} &= \frac{\cos \alpha \sinh 2\xi_0}{Re} \int_0^{2\pi} \zeta_0 \cos(\eta + \alpha) d\eta + \frac{2 \sin \alpha \cosh^2 \xi_0}{Re} \int_0^{2\pi} \zeta_0 \sin(\eta + \alpha) d\eta, \end{aligned} \quad (30a,b)$$

and

$$\begin{aligned} C_{DP} &= \frac{\cos \alpha \sinh 2\xi_0}{Re} \int_0^{2\pi} \left(\frac{\partial \zeta}{\partial \xi} \right)_0 \sin(\eta + \alpha) d\eta - \frac{2 \sin \alpha \cosh^2 \xi_0}{Re} \int_0^{2\pi} \left(\frac{\partial \zeta}{\partial \xi} \right)_0 \cos(\eta + \alpha) d\eta, \\ C_{DF} &= -\frac{2 \cos \alpha \cosh^2 \xi_0}{Re} \int_0^{2\pi} \zeta_0 \sin(\eta + \alpha) d\eta + \frac{\sin \alpha \sinh 2\xi_0}{Re} \int_0^{2\pi} \zeta_0 \cos(\eta + \alpha) d\eta, \end{aligned} \quad (31a,b)$$

where the subscript 0 denotes the cylinder surface $\xi = \xi_0$.

An additional parameter of interest for asymmetric flows is the torque or moment exerted by the fluid upon the cylinder. An expression for the dimensional moment is

$$M^* = \rho d^2 U^2 \oint_C \left\{ (ly - mx) p_0 + \frac{2}{R} (lx + my) \zeta_0 \right\} ds, \quad (32)$$

where the contour of integration is taken round the cylinder surface. The dimensionless moment coefficient is defined by

$$C_M = \frac{M^* R}{\rho d^2 U^2}, \quad (33)$$

and may be decomposed into its pressure and friction components, *i.e.*,

$$C_M = C_{MP} + C_{MF}, \quad (34)$$

where

$$C_{MP} = \int_0^{2\pi} \left(\frac{\partial \zeta}{\partial \xi} \right)_0 \sin^2(\eta + \alpha) d\eta, \quad C_{MF} = \sinh 2\xi_0 \int_0^{2\pi} \zeta_0 d\eta. \quad (35a,b)$$

4. Results

We have confined the analysis to small values of Re, namely $1 \leq \text{Re} \leq 40$, for which the physical problem is expected to exhibit steady-state behaviour. This is supported by the findings of Lugt and Haussling [12] whose results indicate that the unsteady flow past an elliptic cylinder at 45° incidence becomes unstable for $\text{Re} > 45$ (*i.e.*, the solution exhibits vortex shedding). Great care has been taken to ensure the accuracy of these results and comparisons are made to existing results where possible.

Two elliptic cylinders (based on the ratio b/a) are considered. For an elliptic cylinder with $b/a = 1/5$ (*i.e.*, $\tanh \xi_0 = 0.2$), solutions were obtained for Re varying from 1 to 40 and for a range of inclinations α such that $0^\circ \leq \alpha \leq 90^\circ$. A large number of combinations of Re and α in these ranges were considered using the grid $N \times M$, $z_0 = 20 \times 40$, 0.1 (the number of grid points being $N \times 2M = 1600$). This allowed the dependence of the flow solution upon Re and α to be determined. Additional results were obtained for $\text{Re} = 5$ with α varying from 0° to 90° in 10° increments using the grid 20×40 , 0.05, and for $\text{Re} = 20$ using the grids 20×40 , 0.05 and 40×40 , 0.1. Further results were obtained for the case $\text{Re} = 40$, $\alpha = 70^\circ$ using the grids 40×40 , 0.1; 40×40 , 0.05; 40×80 ; 0.01; and 40×80 , 0.05. This allowed a detailed analysis of the grid dependence of the solution to be conducted.

No previous steady-state solutions of the Navier-Stokes equations seem to exist for nonzero values of α for the elliptic cylinder with $b/a = 1/5$. Previous computations have been carried out by Dennis and Chang [24] for this elliptic profile over the range $1 \leq \text{Re} \leq 200$ for $\alpha = 0^\circ$, using a quite different method adapted purely to the case of symmetrical flow. Results obtained here are compared to those of Dennis and Chang for $1 \leq \text{Re} \leq 40$.

The only other results that could be found for steady asymmetric flow past an elliptic cylinder are those of Lugt and Haussling [12]. For an elliptic cylinder with $b/a = 1/10$ (*i.e.*,

Table 1. Comparison of C_D with Dennis and Chang [24] for symmetric flow past an elliptic cylinder.

Re	Present	Dennis and Chang
1	8.096	8.222
5	2.712	—
10	1.765	1.848
20	1.169	1.228
40	0.789	0.794

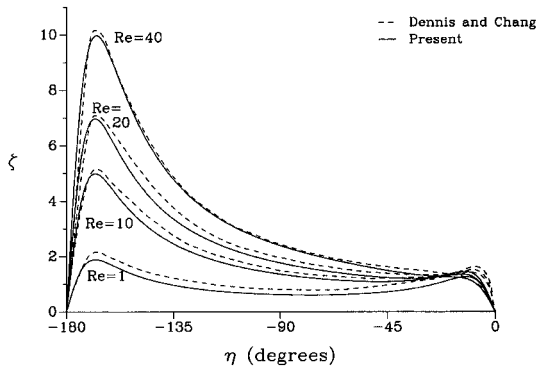


Figure 1. Comparison of surface vorticity for flow past an elliptic cylinder $\tanh \xi_0 = 0.2$ at $\alpha = 0^\circ$.

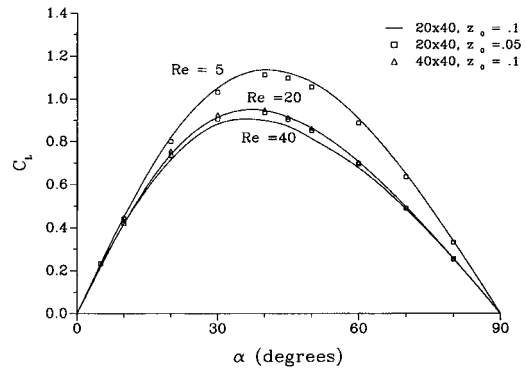


Figure 2. Lift coefficient as a function of incidence for $Re = 5, 20, \text{ and } 40, \tanh \xi_0 = 0.2$.

$\tanh \xi_0 = 0.1$) at 45° incidence to the free stream, they obtained quasi-steady results of the corresponding unsteady problem for $Re = 15$ and 30 . These cases are also considered here and the results compared to Lugt and Haussling.

In Table 1 we compare the $\tanh \xi_0 = 0.2, \alpha = 0^\circ$ results for the drag coefficient C_D with those obtained by Dennis and Chang [24]. The lift coefficient C_L is, of course, zero in this case. The results given are for the 20×40 grid with $z_0 = 0.1$; the significance of z_0 has been noted in the previous section. The comparison seems quite satisfactory, bearing in mind that $z_0 = 0.1$ corresponds to a distance of about 25 times the major axis of the ellipse, whereas Dennis and Chang took their boundary at about $z_0 = 0.19$, which corresponds to approximately 7.5 times the length of the major axis. We have found in this problem that there is a tendency to overestimate the drag if the external boundary is taken too close to the cylinder. Comparison of the vorticity distribution over the surface of the cylinder is made with Dennis and Chang's results in Figure 1. The present surface vorticity is somewhat lower, in general, which accounts in part for the lower estimate of C_D . However, the present results are thought to be the more accurate; this tends to be substantiated by the tests of grid dependence carried out when $\alpha \neq 0^\circ$.

For nonzero inclinations, computations have been carried out for $\alpha = 0^\circ$ to $\alpha = 90^\circ$ by uniform steps of 10° . Various grid structures were used, namely: $20 \times 40, 0.1$; $20 \times 40, 0.05$; and $40 \times 40, 0.1$. One would not expect a great change in the solution as z_0 is reduced from

Table 2. Lift and drag coefficients for the flow past an elliptic cylinder at various angles of incidence to the uniform stream, $Re = 20$ and $\tanh \xi_0 = 0.2$, for various solution grids.

Grid ($N \times M, z_0$)	$20 \times 40,$ 0.05		20×40 0.1		40×40 0.1	
α	C_L	C_D	C_L	C_D	C_L	C_D
20°	0.735	1.295	0.741	1.296	0.758	1.305
40°	0.936	1.598	0.947	1.602	0.951	1.612
60°	0.698	1.904	0.706	1.911	0.703	1.913
80°	0.254	2.084	0.257	2.093	0.253	2.087

0.1 to 0.05 for the same grid structure, provided that these values correspond to sufficiently large ξ for the asymptotic structure to be valid. On the other hand, the change of the basic grid structure from 20×40 to 40×40 may be expected to be significant. Tests of the basic grid size of $\pi/40$ in the η direction were found to be satisfactory due to numerous grid reductions in the wake. Generally speaking, two grid reductions were used for $Re = 5$, three for $Re = 20$, and four for $Re = 40$. In the case of three grid reductions, the grid size in η near $z = z_0$ is made as small as $\pi/320$. The solution process does become more sensitive as Re is increased and requires a greater number of grid reductions. This reflects the more rapid decay of vorticity in the wake for larger Re for which a finer grid is therefore required. Also, results from Lugt and Haussling [12] indicate that, for Re above 45, the unsteady problem does not tend to a steady-state.

The variation of the lift and drag coefficients C_L and C_D with the three grid structures are shown for $Re = 20$ in Table 2 for some selected values of α over the range considered. As noted, the positioning of the boundary $z = z_0$ makes very little difference in the results for the lift coefficient obtained by means of the 20×40 grid and even less in the drag coefficient. Thus the difference between the results on the 20×40 and 40×40 grids is probably a measure of the grid reduction in the z direction and the difference is not great. For example, the maximum difference in the lift coefficient in Table 2, which occurs at $\alpha = 20^\circ$, is about 2.2% and the difference in the drag coefficient is considerably less. The results of comparisons are very similar for $Re = 5$ (for the grids $20 \times 40, 0.1$ and $20 \times 40, 0.05$) and it is hardly necessary to give details in this case. The variation of C_L with α is shown graphically in Figure 2 and the variation of C_D in Figure 3 for $Re = 5, 20$, and 40. The corresponding results for C_L/C_D (grid $20 \times 40, 0.1$) are shown in Figure 4. It may be noted that C_L/C_D increases with Re , which is what Goldstein [25, pp. 450–451] observed for aerofoils at large Re .

Further tests of the grid dependence of the solution for $Re = 40, \alpha = 70^\circ$ were conducted and the results for the lift, drag, and moment coefficients are given in Table 3. The grids considered were $20 \times 40, 0.1$; $40 \times 40, 0.1$; $40 \times 80, 0.1$; $40 \times 40, 0.05$; and $40 \times 80, 0.05$. The results are consistent with the findings noted above for $Re = 20$. The reduction in the η grid size k corresponding to increasing M from 40 to 80 has a greater influence on C_D and C_M (typically 3% to 4%) than on C_L (1% to 2%). Reducing z_0 from 0.1 to 0.05 has a much lower effect (less than 1%).

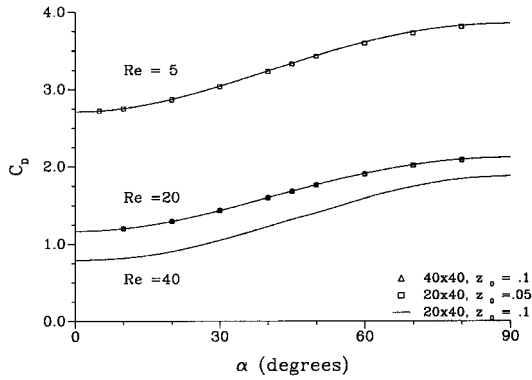


Figure 3. Drag coefficient as a function of incidence for $Re = 5, 20,$ and $40, \tanh \xi_0 = 0.2.$

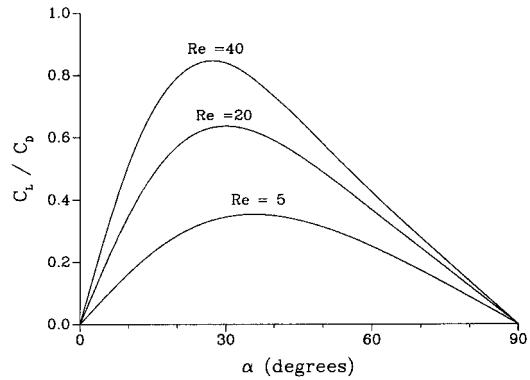


Figure 4. Lift to drag ratio as a function of incidence for $Re = 5, 20,$ and $40, \tanh \xi_0 = 0.2.$

Table 3. Lift, drag, and moment coefficients for the flow past an elliptic cylinder, $Re = 40, \alpha = 70^\circ,$ and $\tanh \xi_0 = 0.2,$ for various solution grids.

Grid ($N \times M, z_0$)	C_L	C_D	$-C_M$
$20 \times 40, 0.1$	0.488	1.741	9.813
$40 \times 40, 0.1$	0.515	1.763	9.510
$40 \times 80, 0.1$	0.508	1.709	9.186
$40 \times 40, 0.05$	0.518	1.766	9.493
$40 \times 80, 0.05$	0.511	1.708	9.116

Table 4. Lift, drag, and moment coefficients, and the error in the surface pressure integration for the flow past an elliptic cylinder ($\tanh \xi_0 = 0.2$) for $Re = 40$ at various angles of incidence to the uniform stream.

α	C_{LP}	C_L	C_{DP}	C_D	$-C_{MP}$	$-C_M$	$ P_0(\pi) - P_0(-\pi) $
0°	$O(10^{-7})$	$O(10^{-7})$	0.156	0.789	$O(10^{-7})$	$O(10^{-7})$	$O(10^{-7})$
10°	0.458	0.419	0.223	0.818	10.23	11.10	0.037
20°	0.779	0.717	0.398	0.904	17.33	18.66	0.036
30°	0.952	0.883	0.643	1.051	20.21	21.60	0.003
40°	0.969	0.900	0.902	1.229	19.64	20.85	0.059
50°	0.881	0.817	1.140	1.405	17.00	17.96	0.096
60°	0.734	0.678	1.368	1.592	13.55	14.26	0.095
70°	0.528	0.488	1.547	1.741	9.325	9.813	0.088
80°	0.276	0.255	1.665	1.841	4.749	4.998	0.053
90°	$O(10^{-7})$	$O(10^{-7})$	1.706	1.876	$O(10^{-7})$	$O(10^{-7})$	$O(10^{-7})$

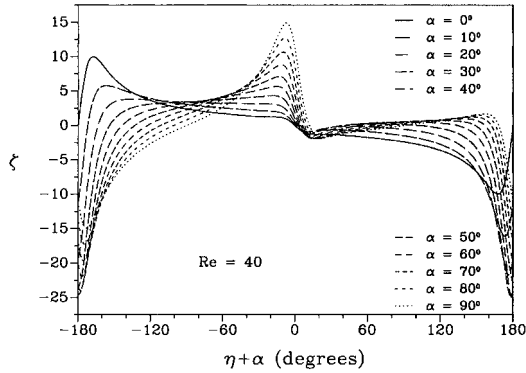


Figure 5. Surface vorticity for an elliptic cylinder $\tanh \xi_0 = 0.2$ at various angles of inclination for $Re = 40$.

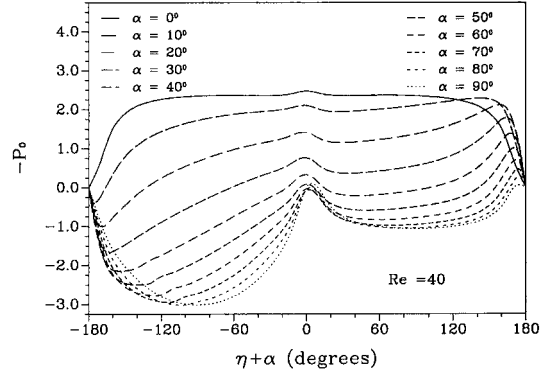


Figure 6. Surface pressure coefficient for an elliptic cylinder $\tanh \xi_0 = 0.2$ at various angles of inclination for $Re = 40$.

In Table 4 we give the complete details of the lift coefficient and its pressure component as a function of α for the typical set of results obtained using the $20 \times 40, 0.1$ grid for $Re = 40$. The frictional component can be obtained by subtracting the pressure component from the lift coefficient. Similar results are given for the drag and moment coefficients in these tables. The pressure component of the lift is positive and larger in magnitude, giving rise to resultant positive lift. The negative frictional lift coefficient can be expected because the frictional force on the cylinder lies along the positive direction of the major axis of the cylinder, which is downwards with respect to the stream velocity. A similar result was obtained by Lugt and Haussling [12] in their calculations of unsteady flow past an elliptic cylinder. The calculated moments on the cylinder are negative and therefore act so as to turn the cylinder broadside to the direction of the stream, consistently with the well-known results of potential theory.

The distribution of dimensionless vorticity over the surface of the cylinder is indicated for $Re = 40$ in Figure 5. Here, $\eta + \alpha = 0$ corresponds to the downstream end of the cylinder and $\eta + \alpha = \pi$ to the corresponding upstream end. Thus, for example, in the two cases $\alpha = 0^\circ$ and 90° in Figure 5 for which the flow is symmetrical about the direction of the stream, the vorticity is anti-symmetrical about $\eta = 0$ and $\eta = \pi/2$, respectively.

The dimensionless surface pressure coefficient defined by the equation

$$P_0 = \frac{4}{R} \int_{\eta_0}^{\eta} \left(\frac{\partial \xi}{\partial \xi} \right)_0 d\eta, \tag{36}$$

where the subscript of the derivative denotes $\xi = \xi_0$, is given as a function of η in Figure 6 for $Re = 40$. The value $\eta_0 = -\pi$ is taken as the base point. The continuity of pressure in completing a circuit was found to be good. The difference $|P_0(\eta_0 + 2\pi) - P_0(\eta_0)|$, found using integration by Simpson's rule, is shown in Table 4 for $Re = 40$ for the $20 \times 40, 0.1$ grid. The maximum error of 0.1 at $\alpha = 50^\circ$ is approximately 4% of the surface pressure at its maximum value. Errors for other inclinations and Re were generally much lower. This verifies that the formulation of the problem which we have adopted does succeed in making the pressure continuous and hence ensures that all the necessary conditions of the problem are satisfied.

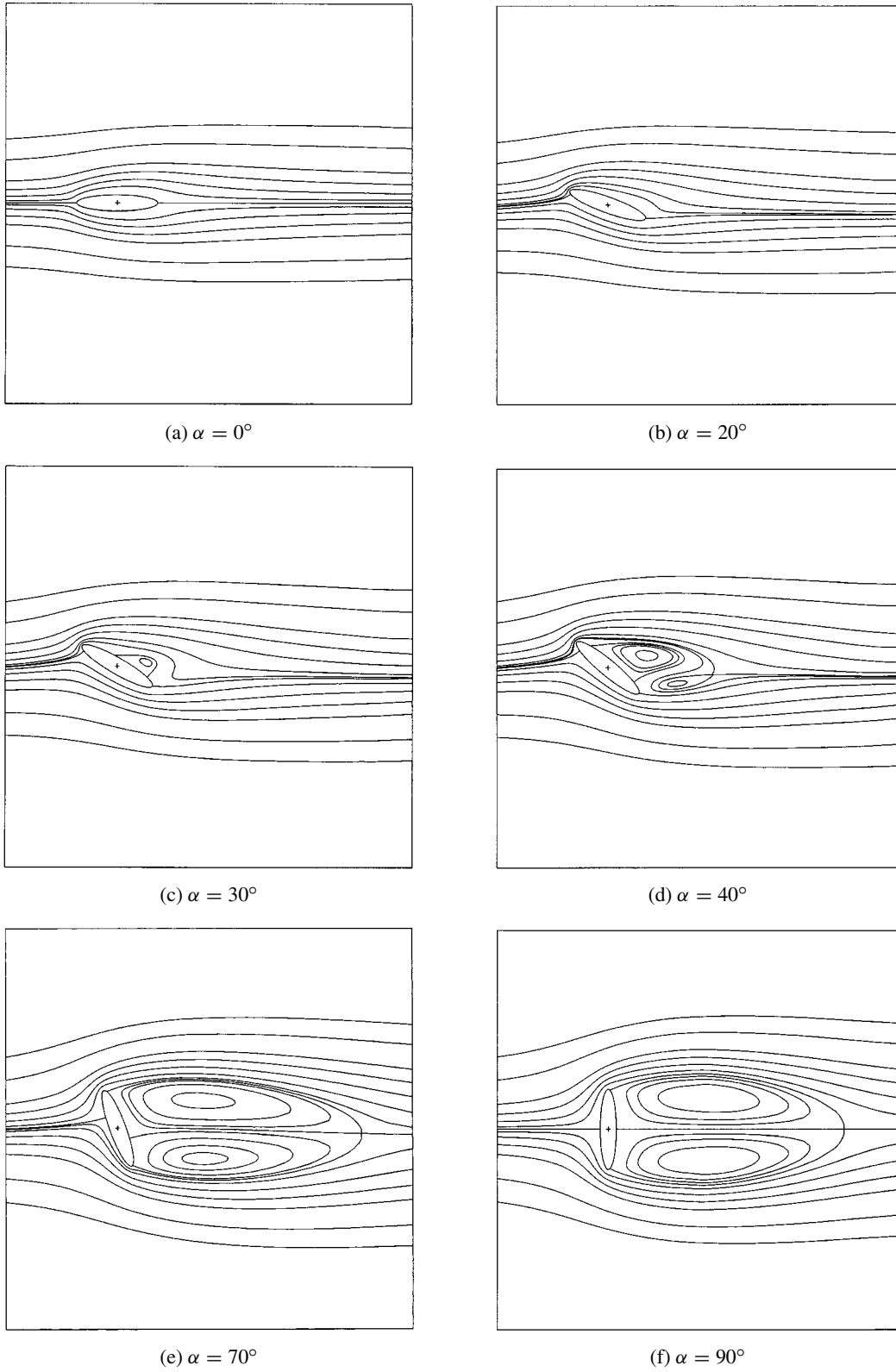


Figure 7. Dimensionless streamlines for $Re = 40$, $\tanh \xi_0 = 0.2$, for various inclinations α .

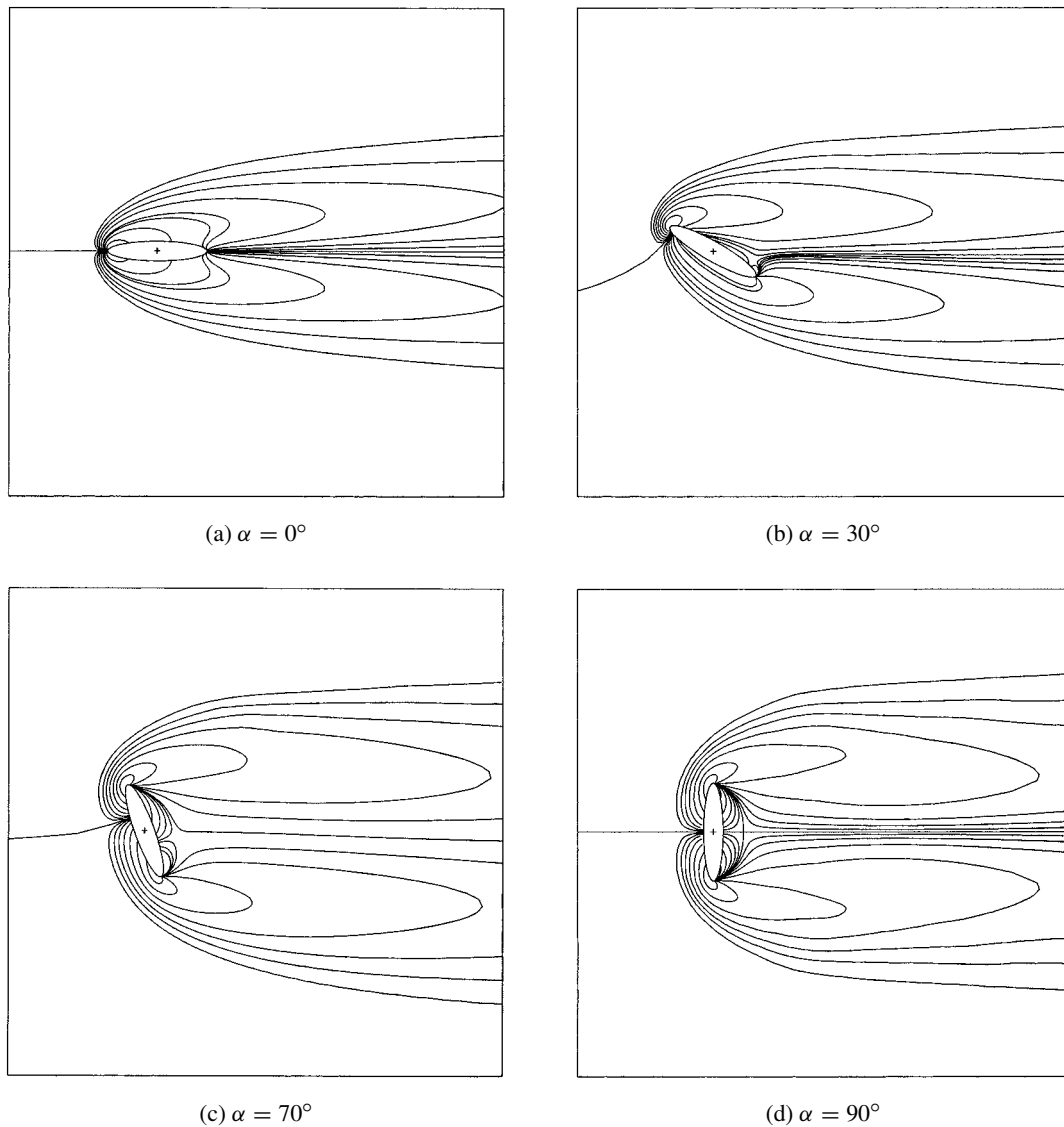


Figure 8. Dimensionless equivorticity lines for $Re = 40$, $\tanh \xi_0 = 0.2$, for various inclinations α .

In most cases the solution has converged by 10,000 iterations, the exception being the more refined $40 \times 80, 0.1$ grid which required upwards of 30,000 iterations for convergence. The $40 \times 80, 0.1$ solution was used as the initial conditions for the $40 \times 80, 0.05$ solution procedure, for which convergence was achieved much faster. In general, coarser solutions were used as initial conditions in obtaining solutions for finer grids. Also, in changing inclination angles, a previous solution for a different inclination was used as the initial conditions.

The streamline patterns of the motion are shown for various values of α in Figure 7 for $Re = 40$. In all cases of Re considered there is no separation of the flow for small values of α ; this is consistent with the calculations carried out by Dennis [19] for the case of Oseen's

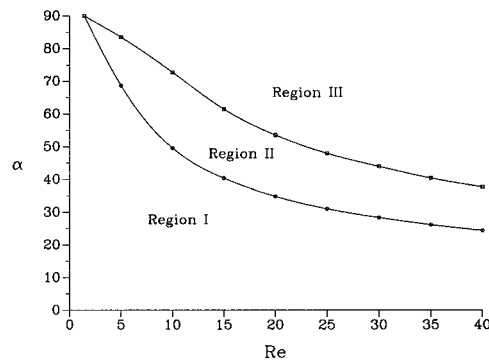


Figure 9. Bifurcation diagram in Re , α space showing regions where, for the elliptic cylinder $\tanh \xi_0 = 0.2$, the solution: I) exhibits no separation; II) has separation with a single attached recirculatory region; and III) has separation with two recirculatory regions.

linearised equations. As α increases, separation occurs and it occurs for smaller values of α for Re increasing. In all cases a single separation bubble forms which grows as α increases. Eventually this bubble must form into two counter rotating vortices present in the case $\alpha = 90^\circ$ (Figure 7f). Some indication of how this happens is given in Figures 7c, d, and e for $Re = 40$. Once the initial separation bubble (which is attached to the cylinder) has formed, further increases in inclination cause it to grow. This is accompanied by the development and growth of a second stagnant region below the bubble. At some inclination this stagnant region is pinched off with the appearance of a saddle point in the stream function, and a second recirculatory region unattached to the cylinder is formed. With further increases in inclination the two recirculatory regions grow until the symmetric flow for $\alpha = 90^\circ$ is achieved. These results are in agreement with the speculation by Smith [26] for flow development past a thin aerofoil as the angle of incidence is increased. Smith shows, for a flat plate with angle of incidence increasing to 90° , growth of a single attached recirculatory region following by the appearance of a second, initially unattached, recirculatory region. This second recirculatory region attaches near but before incidence of 90° . Once normal to the free stream, a flow pattern similar to Figure 7f is achieved.

Equivorticity lines for various values of α for $Re = 40$ are shown in Figure 8. The change in vorticity patterns which accompanies the change in streamlines as α approaches 90° is again quite interesting.

The results obtained for $Re = 5, 20$ and 40 indicate that the solutions fall into three classes (for the range of Re studied). For small inclinations there is no separation, for medium inclination there is separation with a single attached recirculatory region (bounded by the streamline $\psi = 0$), and for large inclinations there is separation with two recirculatory regions (a second unattached region forming that is bounded by ψ_{SdPt} , the streamline through a saddle point). As the Reynolds number increases the angles at which each of these recirculatory regions first appears decrease. Further runs were done at $Re = 5, 10, 15, \dots, 40$, grid $20 \times 40, 0.1$ ($\tanh \xi_0 = 0.2$) to determine the angles (to the nearest tenth of a degree) at which each of the recirculatory regions first appears for a given Re . Runs were also done at $\alpha = 90^\circ$ for $Re < 5$ to determine at which Re separation first occurs for this inclination (found to be $Re = 1.45$). These results were used to construct the bifurcation diagram given in Figure 9 showing the three regions of the solution for $Re \leq 40$. The figure clearly shows both recirculatory regions first appearing at decreasing angles of incidence as Re increases. Dennis and Chang [24] have

Table 5. Lift, drag, and moment coefficients, and the error in the surface pressure integration for the flow past an elliptic cylinder ($\tanh \xi_0 = 0.1$) for $\text{Re} = 15$, $\alpha = 45^\circ$.

Grid ($N \times M, z_0$)	C_{LP}	C_L	C_{DP}	C_D	$-C_{MP}$	$-C_M$	$ P_0(\pi) - P_0(-\pi) $
$20 \times 40, 0.1$	1.275	1.018	1.350	1.821	8.479	8.850	0.095
$40 \times 40, 0.1$	1.182	0.918	1.262	1.737	8.450	8.803	0.256
$40 \times 80, 0.1$	1.324	1.067	1.400	1.871	8.423	8.795	0.011
$80 \times 80, 0.1$	1.322	1.065	1.399	1.870	8.410	8.781	0.011
$40 \times 40, 0.05$	1.173	0.908	1.253	1.730	8.426	8.774	0.262
$40 \times 80, 0.05$	1.313	1.050	1.391	1.865	8.410	8.769	0.003

found that, for $\alpha = 0^\circ$, separation first occurs for Re less than but near 200. It is expected that the boundaries separating the regions in Figure 9 will decrease in α for increasing Re , converging to $\alpha = 0^\circ$ at some Re near 200. Above this Re the solution is expected to contain two recirculatory regions for all inclinations.

For $\text{Re} = 20$, the formation of the second, unattached, recirculatory region occurs with the appearance of a saddle point in the stream function at $\alpha \sim 54^\circ$. The value of the streamline through this saddle point is initially small and positive, *e.g.* for $\alpha = 60^\circ$, $\psi_{\text{sdPt}} = 0.0284$. As the inclination approaches 90° , ψ_{sdPt} decreases monotonically to zero. For $\text{Re} = 40$ the development of the recirculatory regions with increasing incidence is more complicated. When the saddle point first appears ($\alpha = 37.7^\circ$) it is small and positive. As α increases further ψ_{sdPt} decreases until at $\alpha \sim 57^\circ$ it equals zero. For larger inclinations ψ_{sdPt} becomes negative decreasing and then increasing to zero as α approaches 90° . Figures 7d and e show the differences in the streamline patterns for ψ_{sdPt} positive *vs.* negative. For $\alpha < 57^\circ$ the upper recirculatory region is attached to the cylinder while the lower is unattached (see Figure 7d for $\alpha = 40^\circ$). At $\alpha \sim 57^\circ$ both recirculatory regions are attached (similar to Figure 6h of Lugt and Haussling [12]). For $\alpha > 57^\circ$ the lower recirculatory region is now attached with the upper being unattached (until the inclination equals 90° , see Figure 7e for $\alpha = 70^\circ$). This result indicates the possibility of a fourth region on the bifurcation diagram of Figure 9. In this region the attached recirculatory bubble is the lower of the two as exemplified by the high incidence results for $\text{Re} = 40$ when ψ_{sdPt} is negative. Lugt and Haussling's time dependent results for $\text{Re} = 30$, $\alpha = 45^\circ$, $\tanh \xi_0 = 0.1$ show a converging solution (for large time) in which the attached recirculatory region oscillates between the upper and lower. The transitions are not accompanied by any vortex shedding.

Solutions were obtained for an elliptic cylinder with $\tanh \xi_0 = 0.1$, for $\text{Re} = 15$ and 30 , $\alpha = 45^\circ$ using the grids ($N \times M, z_0$): $20 \times 40, 0.1$; $40 \times 40, 0.1$ and 0.05 ; $40 \times 80, 0.1$ and 0.05 ; and $80 \times 80, 0.1$. These cases allow comparison of steady-state results obtained from the methodology presented here with the results obtained by Lugt and Haussling [12]. Three grid reductions are performed for $\text{Re} = 15$ and four for $\text{Re} = 30$.

In Table 5, results for the lift; drag and moment coefficients, and the surface pressure error are presented for $\text{Re} = 15$, $\alpha = 45^\circ$ for the six grid solutions. Similar results for $\text{Re} = 30$, $\alpha = 45^\circ$ are presented in Table 6. These results illustrate different shifts as the grid sizes are varied. Increasing M from 40 to 80 when $N = 40$ causes a 10% to 15% change in C_L , with smaller changes for the other coefficients. Conversely, doubling N from 40 to 80 when

Table 6. Lift, drag, and moment coefficients, and the error in the surface pressure integration for the flow past an elliptic cylinder ($\tanh \xi_0 = 0.1$) for $Re = 30$, $\alpha = 45^\circ$.

Grid ($N \times M, z_0$)	C_{LP}	C_L	C_{DP}	C_D	$-C_{MP}$	$-C_M$	$ P_0(\pi) - P_0(-\pi) $
$20 \times 40, 0.1$	1.145	1.029	1.183	1.452	14.93	15.60	0.112
$40 \times 40, 0.1$	0.999	0.862	1.050	1.329	14.40	14.88	0.174
$40 \times 80, 0.1$	1.079	0.945	1.130	1.408	14.31	14.80	0.020
$80 \times 80, 0.1$	1.076	0.941	1.128	1.406	14.25	14.74	0.027
$40 \times 40, 0.05$	0.986	0.847	1.039	1.320	14.40	14.87	0.189
$40 \times 80, 0.05$	1.069	0.930	1.121	1.402	14.35	14.82	0.004

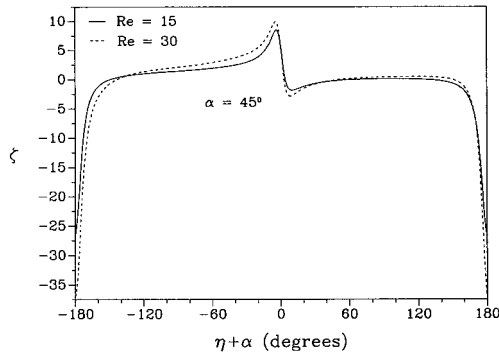


Figure 10. Surface vorticity for flow past an elliptic cylinder $\tanh \xi_0 = 0.1$ for $Re = 15$ and 30 , $\alpha = 45^\circ$.

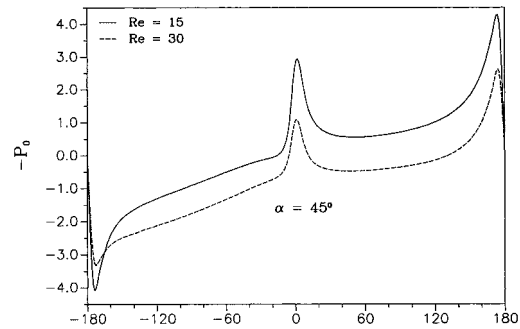


Figure 11. Surface pressure coefficient for flow past an elliptic cylinder $\tanh \xi_0 = 0.1$ for $Re = 15$ and 30 , $\alpha = 45^\circ$.

$M = 80$ has less than 1% effect on all coefficients. Reducing z_0 from 0.1 to 0.05 results in changes of 0.2% to 1.6% to the coefficients. The error in continuity of the surface pressure significantly reduces when M is increased from 40 to 80. When compared to Table 3 for the $\tanh \xi_0 = 0.2$ elliptic cylinder, these results for the thinner cylinder indicate a greater sensitivity to the η grid size. The results for $M = 40$ are now not as accurate when compared to finer grids as they were for the $\tanh \xi_0 = 0.2$ cylinder. This could perhaps be expected as the thinner elliptic cylinder profile is closer to that of a flat plate for which singularities exist at the leading and trailing edges. Given the numerical schemes are $O(h^2)$ and $O(k^2)$ accurate, grid dependence of the solutions are expected. The results presented here do indicate decreasing changes as the grids are reduced. It would be possible to perform h^2 and k^2 extrapolation if further grid solutions were obtained.

Surface vorticity plots for $Re = 15$ and 30 are shown in Figure 11 while Figure 12 presents the surface pressure distributions. In both figures $80 \times 80, 0.1$ grid solutions were used. Streamline and equivorticity line plots for the two cases are shown in Figures 13a,b and 14a,b. The streamline plot for $Re = 15$ has a single attached recirculatory region while that for $Re = 30$ has two recirculatory regions, one attached and one unattached. Comparison

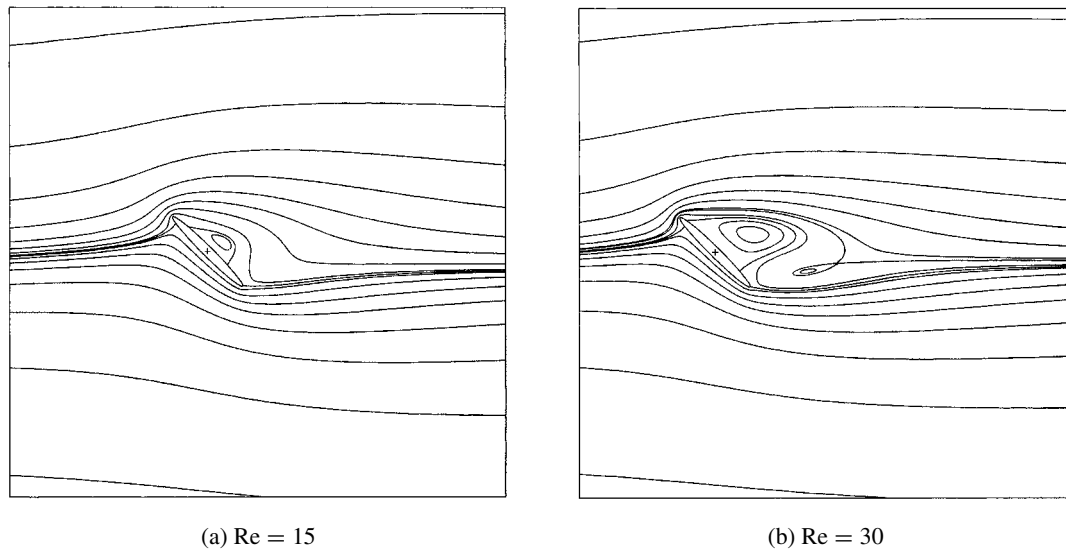


Figure 12. Dimensionless streamlines for the elliptic cylinder $\tanh \xi_0 = 0.1$ at $\alpha = 45^\circ$ incidence to the uniform stream.

Table 7. Lift, drag, and moment coefficients as a function of time for the unsteady flow past an elliptic cylinder ($\tanh \xi_0 = 0.1$, $\alpha = 45^\circ$), from Lugt and Haussling [12].

Re	t	C_L	C_D	C_M
15	5.39	1.37	2.21	10.6
	6.39	1.32	2.15	10.3
30	18.0	0.955	1.45	15.2
	20.2	0.940	1.44	15.2

of these plots to those from Lugt and Haussling (at the largest time considered) shows good agreement.

Table 7 presents lift, drag, and moment coefficients for the last two reported times from Lugt and Haussling, for $Re = 15$ and 30 , $\alpha = 45^\circ$ (results transferred to present definitions). For $Re = 15$, $\alpha = 45^\circ$, Lugt and Haussling's results have not completely converged as is indicated in Table 7 (the lift, drag, and negative moment still decreasing). At the largest time (6.39 nondimensional units) these results compare to the 80×80 , 0.1 grid results as follows (Lugt and Haussling vs. present): C_L : 1.32 vs. 1.065; C_D : 2.15 vs. 1.870; and C_M : 10.3 vs. 8.781 (differences being 24%, 15%, and 17%, respectively). For $Re = 30$, $\alpha = 45^\circ$ (for which Lugt and Haussling have taken their solution further in time, *i.e.*, 20.2 nondimensional units) the comparison is much better: C_L : 0.940 vs. 0.941; C_D : 1.44 vs. 1.406; and C_M : 15.2 vs. 14.74 (differences being 0.1%, 2.4%, and 3.1%, respectively).

5. Conclusions

In the present paper we have investigated the steady flow past an elliptic cylinder at various inclinations to the stream by means of numerical solutions of the Navier-Stokes equations. The calculations have been restricted to low values of the Reynolds number for which the physical problem is expected to be stable. Complete results have been obtained for the $\tanh \xi_0 = 0.2$ elliptic cylinder for inclinations in the range zero to 90° and Re varying up to 40. For small inclinations the lift to drag ratio varies approximately linearly with inclination and there is no separation of the flow. With increasing inclination separation eventually occurs and the lift to drag ratio decreases. The results demonstrate how, as the inclination increases from zero to 90° , the streamline patterns change from the symmetric flow at 0° inclination, through asymmetric flows with either no separation, separation with a single recirculating region, or separation with two recirculating regions, to the symmetric flow at 90° with two attached vortices. A bifurcation diagram illustrating this solution behaviour was constructed for $Re \leq 40$. These results indicate fluid behaviour that, to our knowledge, has not been noted before (but is alluded to by the unsteady results of Lugt and Haussling [12]), namely steady-state asymmetric flow in which there are two recirculatory regions behind the cylinder, one attached and one unattached to the cylinder.

To validate the methodology used in this paper, results were also obtained for the cases considered by Lugt and Haussling ($\tanh \xi_0 = 0.1$ elliptic cylinder at $Re = 15$ and 30 , $\alpha = 45^\circ$). Their results, although not taken far enough in time for true steady-state behaviour (especially for the $Re = 15$ case), compare favourably with our results and support the findings regarding separation for asymmetric flows.

One of the main objectives of this study has been to point out that the conditions at large distances must be carefully considered in order to obtain satisfactory solution procedures. The present method using the transformations (23) appears to give satisfactory results but further investigations of problems in which lift and circulation are present seem to be necessary. Fornberg [23] has investigated alternative outer boundary conditions for the symmetrical flow past a circular cylinder for Reynolds numbers up to 300. The derivative condition $\partial\zeta/\partial\xi = 0$ was used for the vorticity. Fornberg considered the following alternatives for the stream function: first term of the Oseen approximation (equivalent to that used here), free stream ($\psi = 0$), normal derivative zero ($\partial\psi/\partial\xi = 0$) and a mixed condition. The normal condition was found to give best results for Reynolds numbers up to 40 while the mixed condition was better for larger Reynolds numbers. It would be useful to expand upon the asymmetric investigation presented here to consider alternative methods for imposing boundary conditions at large distances. It must be noted, however, that the asymmetric problem introduces new complexities over the symmetrical problem, namely, the rapid decay of the vorticity must be achieved in order to ensure a correct solution is found.

References

1. H. Hasimoto, On the flow of a viscous fluid past an inclined elliptic cylinder at small Reynolds numbers. *J. Phys. Soc. Japan* 8 (1958) 653–661.
2. S.C.R. Dennis and S. Kocabiyik, The solution of two-dimensional Oseen flow problems using integral conditions. *IMA J. Appl. Math.* 45 (1990) 1–31.
3. H. Mizomoto, A note on the numerical treatment of Navier-Stokes equations. I. *J. Phys. Soc. Japan* 34 (1973) 1396–1401.

4. Ta P. Loc, Étude numérique de l'écoulement d'un fluide visqueux incompressible autour d'un cylindre fixe ou en rotation. Effet Magnus. *J. Mécanique* 14 (1975) 109–133.
5. D.B. Ingham, Steady flow past a rotating cylinder. *Comp. Fluids* 11 (1983) 351–366.
6. H.M. Badr, S.C.R. Dennis and P.J.S. Young, Steady and unsteady flow past a rotating circular cylinder at low Reynolds numbers. *Comp. Fluids* 17 (1989) 579–609.
7. D.B. Ingham and T. Tang, A numerical investigation into the steady flow past a rotating circular cylinder at low and intermediate Reynolds numbers. *J. Comp. Phys.* 87 (1990) 91–107.
8. T. Tang and D.B. Ingham, On steady flow past a rotating circular cylinder at Reynolds numbers 60 and 100. *Comp. Fluids* 19 (1991) 217–230.
9. S.J.D. D'Alessio and S.C.R. Dennis, A vorticity model for viscous flow past a cylinder. *Comp. Fluids* 23 (1994) 279–293.
10. S.J.D. D'Alessio and S.C.R. Dennis, Steady laminar forced convection from an elliptic cylinder. *J. Eng. Math.* 29 (1995) 181–193.
11. F.T. Smith and S.C.R. Dennis, Computations on flow past an inclined flat plate of finite length. *J. Eng. Math.* 24 (1990) 311–321.
12. H.J. Lugt and H.J. Haussling, Laminar flow past an abruptly accelerated elliptic cylinder at 45° incidence. *J. Fluid Mech.* 65 (1974) 711–734.
13. P.K.G. Panniker and Z. Lavan, Flow past impulsively started bodies using Green's functions. *J. Comp. Phys.* 18 (1975) 46–65.
14. V.A. Patel, Flow around the impulsively started elliptic cylinder at various angles of attack. *Comp. Fluids* 9 (1981) 435–462.
15. U.B. Mehta and Z. Lavan, Starting vortex, separation bubbles and stall: a numerical study of laminar unsteady flow around an airfoil. *J. Fluid Mech.* 67 (1975) 227–256.
16. S.C.R. Dennis, P. Nguyen and S. Kocabiyik, The flow induced by a rotationally oscillating and translating circular cylinder. *J. Fluid Mech.* 407 (2000) 123–144.
17. R. Kahawita and P. Wang, Numerical simulation of the wake flow behind trapezoidal bluff bodies. *Comp. Fluids* 31 (2002) 99–112.
18. H.M. Badr and S.C.R. Dennis, Time-dependent viscous flow past an impulsively started rotating and translating circular cylinder. *J. Fluid Mech.* 158 (1985) 447–488.
19. S.C.R. Dennis, The computation of two-dimensional asymmetrical flows past cylinders. *Comp. Fluid Dyn. SIAM-AMS Proc.* 11 (1978) 156–177.
20. P.J.S. Young, Steady asymmetric flow of a viscous fluid past a cylinder. Ph.D. Thesis, University of Western Ontario, London, Ontario, Canada (1989) 139pp.
21. I. Imai, On the asymptotic behaviour of viscous fluid flow at a great distance from a cylindrical body, with special reference to Filon's paradox. *Proc. R. Soc. London A*208 (1951) 487–516.
22. L.C. Woods, A note on the numerical solution of fourth order differential equations. *Aeronaut. Q.* 5 (1954) 176–184.
23. B. Fornberg, A numerical study of steady viscous flow past a circular cylinder. *J. Fluid Mech.* 98 (1980) 819–855.
24. S.C.R. Dennis and G.Z. Chang, Numerical integration of the Navier Stokes equations in two dimensions. Mathematics Research Center, University of Wisconsin, *Technical Summary Report* No. 859. (1969) 89pp.
25. S. Goldstein (Ed.), *Modern Developments in Fluid Dynamics Volume II*, New York: Dover Publications, Inc. (1965) 702pp.
26. F.T. Smith, Interacting flow theory and trailing edge separation – no stall. *J. Fluid Mech.* 131 (1983) 219–249.